Fresenius J Anal Chem (1997) 358 : 25–31

INVITED LECTURE

K. Wetzig · S. Baunack · V. Hoffmann · S. Oswald
F. Präßler

Quantitative depth profiling of thin layers

Received: 24 June 1996 / Revised: 10 January 1997 / Accepted: 14 January 1997

Abstract Foundations of sputtering profile evaluation are discussed, which allow the conversion of a measured sputtering profile, I = f(t), to a true element concentration profile $c_{elem.}$ = f(z), or in special cases to a phase profile c_{phase} = f(z). As a relatively new method for quantitative thin film analysis, glow discharge optical emission spectrometry (GDOES) has the special advantage of a narrow depth resolution function. Growing sputter crater profiles can be eliminated by a deconvolution algorithm, as is shown for TiN/TiAlN multilayers. The sputtering rate as a function of depth may be also deduced by a special wedge crater profile, which is sputtered into the material by an ion beam under suitable beam control. Further information on a phase depth profiling may be obtained by principal component analysis, as is discussed for AES and XPS investigations of P implanted Ti. A special technique of cross section imaging of thin layers is the analytical TEM, which allows the parallel investigation of microstructure and element distribution, as illustrated for a Cr-Fe multilayer.

1 Introduction

Thin layers and their structural and chemical characterization have become more and more important during recent years. This concerns, for example, gradient layers and alternating layers in multilayer systems. Also the understanding of interface structures is of growing interest. These arrangements are not only determined by the depth profile of element concentrations but also by that of phase concentrations, as it can be evaluated by modern principal component analysis. Because thin films down to monolayers are of growing interest, problems of layer influence during sputtering by mixing, implantation and similar processes become more and more awkward. From these problems follows the demand for a low information depth and for a good depth profile resolution down to one monolayer.

As to the obtained depth profile I(t) or c(z), modern methods for depth profiling may be divided into 4 groups:

1. The surface layer is uncovered by ion sputtering and then analyzed by means of Auger- or photoelectron spectrometry (AES, XPS).
2. The sputtered part of the surface is immediately used for depth profile analysis. This is the case for secondary ion and sputter neutral mass spectrometry (SIMS, SNMS) and for glow discharge optical emission spectrometry (GDOES).
3. Non-destructive depth profiling methods as total reflection X-ray fluorescence (TXRF) and Rutherford backscattering (RBS).
4. A special method is the analytical TEM (ATEM), which allows section analysis by EDXS and EELS after a complicated sample preparation.

Each of these methods has special advantages. AES combines a depth resolution of only few nm with best lateral resolution values of about 20 nm [1]. The main advantage of XPS is the possibility to obtain chemical bonding information. Trace analyses down to hydrogen (Z = 1) with detection limits below the ppm range can be obtained with SIMS and SNMS. GDOES is a quick method with sputtering rates up to 100 nm/s [2], that does not need high vacuum. On the other hand, one must renounce microscopic lateral resolution. The special advantage of cross-section analysis in ATEM lies in its excellent layer depth resolution, which acts here as lateral resolution with values of few nm.

K. Wetzig (✉) · S. Baunack · V. Hoffmann · S. Oswald
F. Präßler
Institut für Festkörper- und Werkstofforschung Dresden,
Institut für Festkörperanalytik und Strukturforschung,
Postfach 27 00 16, D-01171 Dresden, Germany

2 Evaluation of concentration – depth profiles

The following expositions shall be limited to sputtering methods as AES, XPS, SIMS, SNMS and GDOES. The

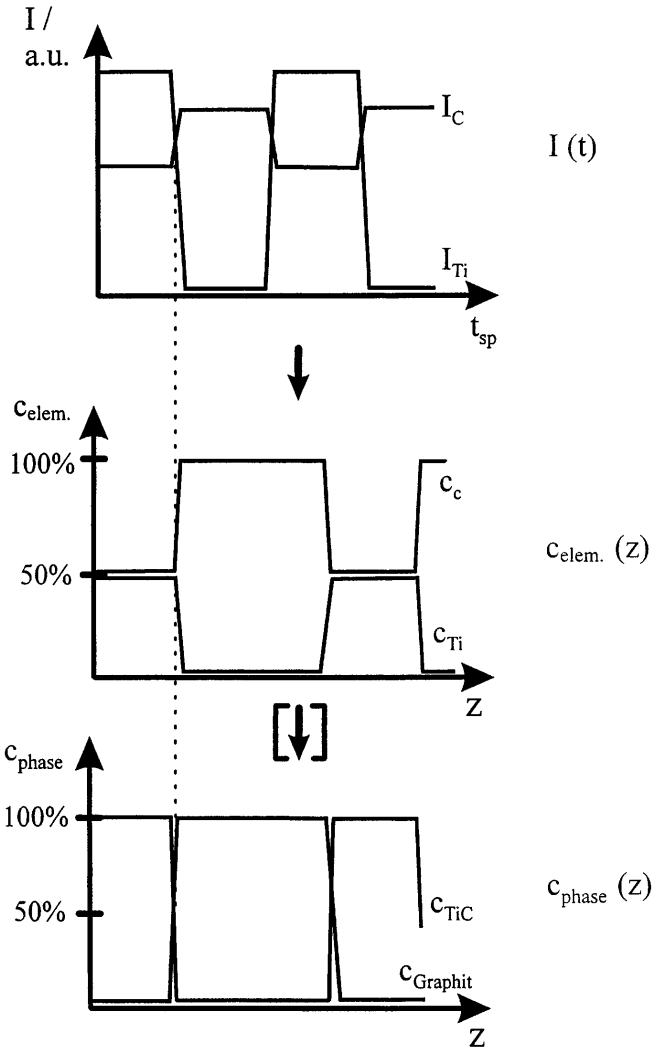

Fig. 1 Determination of concentration-depth profiles for a TiC-C multilayer system (schematically)

concentration-depth profile c = f(z) must be evaluated from the measured intensity-time profile I = f(t). Generally, c is the element concentration, but in some cases it can also be interpreted as a phase concentration, because of different bonding states, resulting in different peak shapes. Figure 1 illustrates these facts for a TiC-C multilayer system. Because C exists in both phases, C and TiC, its element concentration $c_{elem.}(z)$ is always different from zero. An interesting fact is the non-linear transformation from the t-axis to the z-axis because of different sputtering rates of the individual layers. The phase-depth profile interprets the real C concentrations in the alternating TiC and graphitic C layers.

Two steps are necessary to receive the c(z) profile from the measured I(t) profile:

– depth calibration z = f(t),
– elemental or phase concentration calibration c = f(I).

The sputtering process results in a variation of composition and morphology of the surface layer which must be taken into account to reveal the true profile c = f(z) [3]. The eroded depth z is determined by the sputtering rate ż according to

$$z(t) = \int_0^t \dot{z}dt. \quad (1)$$

Assuming a constant sputtering rate, (1) can be written as

$$\dot{z} = \frac{z_o}{t_o} = \text{const.} \quad (2)$$

and the calibration is carried out by a crater depth measurement. However, usually ż varies with composition and the relation between sputtering time and depth becomes non-linear. Even for a constant composition the sputtering rate changes until the dynamic equilibrium is reached. Therefore ż must be measured during the sputtering process, e. g. by in situ laser interferometry.

For multicomponent targets, in the simplest case a binary system A/B, the sputtering process is determined by the sputtering yields Y_A, Y_B, depending on both A and B components. In the steady state the mass fluence of the components A and B is proportional to their concentrations, however the surface concentration may differ from the bulk value as the ratio Y_A/Y_B is not equal to 1 (so-called preferential sputtering) [4–6].

The preferential sputtering and the electron escape depth, both limit the concentration calibration for methods investigating the remaining surface material (AES, XPS). Because both depth dependences are in the same order of magnitude – some nm – this task can only be solved for some special cases [7]. For methods that analyze sputtered material directly (GDOES, SIMS, SNMS) the proportionality between mass flux and concentration can be advantageously used if material density and sensitivity factors are known.

An important parameter for the accuracy in the depth profile is the depth resolution Δz, due to surface roughening, atomic mixing and sputtering parameters [8]. Its value must be minimized. Because of the non-directed and low energetic sputtering process a narrow depth resolution function is available with plasma SNMS and with GDOES.

3 Depth profiling by GDOES

Therefore, in the recent time GDOES has been proved to be a very useful technique for fast depth profile analysis of thin layers and layer systems. In a glow discharge spectral emission line intensities of all sample constituents are measured simultaneously during the sputtering process. Afterwards, the measured intensity-time profiles have to be converted for quantitative analysis into concentration-depth profiles. For that purpose the quantification by Bengtson [9] is commonly used very successfully.

Generally, for a quantification procedure in GDOES mostly two important concepts are used. Firstly, using the concept of constant emission yields, i.e. at constant

plasma parameters the measured intensities I_i are assumed to be proportional to the concentration of the elements in the plasma, the concentration of the elements in the sample can be calculated as a function of the sputtering time. The corresponding basic equation (3) is independent of the matrix type and therefore especially suitable for quantification of layer structures. The emission yield S_i and its dependence on the discharge parameters, described by an excitation function E_i, are determined during a calibration procedure using certified reference material with known concentrations c_i and sputtering rates q:

$$I_i = q \cdot c_i \cdot E_i \cdot S_i \qquad (3)$$

Secondly, the achieved depth can be determined according to the concept of integrated intensities, which means that the integrated intensities correspond to the total sputtered mass. For the calculation of depth, the partial densities of the elements in the sample must be known, e.g. by X-ray diffraction methods, or estimated from a suitable density or lattice model.

Measured intensity-time profiles are affected in GDOES as in other related analytical methods by the shape of the erosion crater during sputtering. The resulting depth resolution suffers from these crater effects since it is impossible to optimize the discharge parameters to an ideally flat crater shape. Therefore, it is a substantial improvement by Präßler et al. [10] for the quantification procedure to implement in the time-to-depth transformation information on the crater formation process. The introduced iterative deconvolution technique takes numerically into consideration for the calculation of the signal response:

1. The sputtering process can be described by an ion current density distribution function, which is independent of time and rotationally symmetrics.
2. The measured intensity is among others proportional to the actually sputtered area of the appropriate layer.
3. The signal response depends on the transfer of sputtered particles into the plasma. That means, particles sputtered at the crater edge will be detected only with the intensity half of that of particles sputtered in the crater center [11].

For the relation of sputtering time and depth it is assumed that the true mass-depth profile is linearly convoluted by a two-dimensional function on to the measured mass-time profile (for details see [10]). The matrix elements of this function can be calculated using the assumptions mentioned above and the measured final crater shape. Because the sputtering process and thereby the time-to-depth transformation itself depend very strongly on the unknown layer structure, the calculation of the matrix elements must be improved iteratively.

In [10] the mathematical handling was demonstrated for the analysis of a multilayer sample with sharp concentration profiles. The achieved improvement was qualitatively shown by the comparison of concentration-depth profiles with and without deconvolution technique.

Because of a non-Gaussian relation for the signal response, the quantitative evaluation of depth resolution in GDOES may be carried out using:

$$\Delta z = \Delta c / \left(\frac{dc}{dz} \right)_{max} \qquad (4)$$

Whereas the depth resolution in Fig. 2 grows in a straight line up to 80 nm in 1 µm depth, it remains constant at 20 nm using the deconvolution technique. That means, the depth resolution and thereby also the quantification become then almost independent of the sputtering depth.

Similar results were achieved by application of the deconvolution algorithm to the analysis of applied materials. Figure 3 shows the intensity-time profile of a 4 µm thick TiN/TiAlN multilayer system made by PA-CVD. Because of the curved crater shape, the depth resolution decreased with increasing depth. The comparison of the concentration-depth profiles in Fig. 4 clearly demonstrates that the differentiation between real concentration gradients and the influence of crater effects is only possible by use of the deconvolution technique. The deconvoluted profile confirms constant concentration ratios in the multilayer

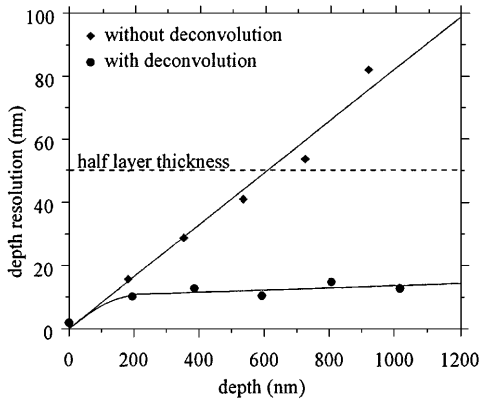

Fig. 2 Comparison of the depth resolution of a Cu/CrNi multilayer system [10] with and without deconvolution technique (discharge gas: Ar, gas pressure: 770 Pa)

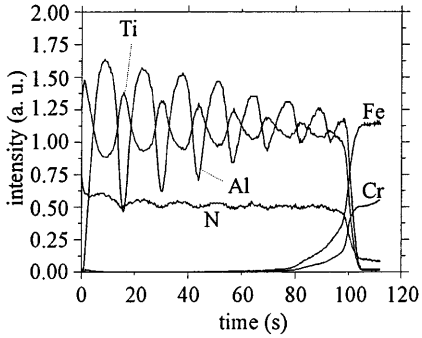

Fig. 3 Intensity-time profile of a hard-coating multilayer system of TiN/TiAlN. The depth resolution becomes worse with increasing depth because of crater effects (discharge gas: Ar, gas pressure: 770 Pa)

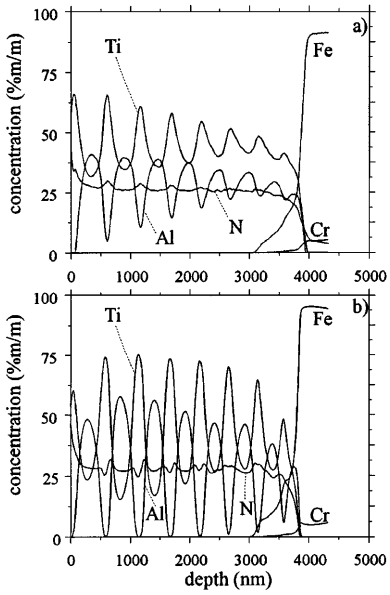

Fig. 4a, b Calculated concentration-depth profiles of the I(t)-profile in Fig. 3. **a)** without deconvolution technique, **b)** with deconvolution technique

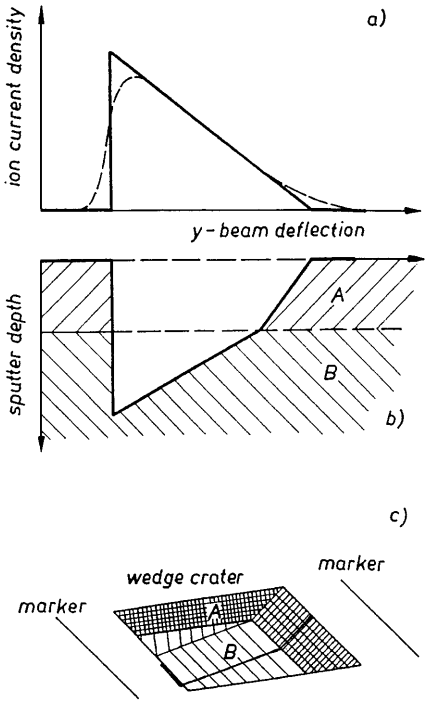

Fig. 5a–c Wedge crater sputtering technique. **a)** Ion current density, **b)** Sputter depth in a two-layer system, **c)** Wedge crater topography

structure. Finally, due to the roughness of the steel surface of about 0.5 µm, no sharp interface to the substrate exists.

As a result, with GDOES it is possible to calculate the concentration-depth profile from the measured intensity-time behaviour: For that purpose, at the beginning the total sputtered mass per time is determined from the total intensities and by inclusion of the density the erosion rate, i.e. the depth of erosion per time, is achieved. This procedure is also known from SNMS [12], but cannot be transferred to most other sputtering techniques, because of the matrix effect (SIMS) or the measurement at the remaining surface (AES, XPS).

4 Wedge crater sputtering

An effective method for the determination of the sputter rate-depth function of complex layer systems with only one sputtering experiment is the so-called "wedge crater sputtering" proposed by Voigtmann [13]. The principle is based on the sputtering of a bevelled crater prepared by a computer controlled saw-tooth like current density profile of the sputtering ion beam. Thus a two layer system with different sputter rates is reflected by a crater bottom with two different slopes (see Fig. 5), which may be determined by a surface profilometer measurement. Main advantage of such a bevelling experiment is that the ion beam parameters are very close to that used in the depth profiling measurement.

In the real case, in general, some further facts have to be considered:

– the real ion beam profile is not an ideal saw tooth (see also Fig. 5) because of the limited diameter of the used ion beam,
– an exact digitalized surface profilometer measurement has to be used,
– the sputter-rate depth function results from the solution of an integral equation.

To consider this, a crater shape simulation program first established for the consideration of crater distortion in SIMS [14] was modified for the purpose of the proposed experimental set-up [15].

As Fig. 6 shows, further problems occur if the procedure is used for investigations at real world samples (e.g. layer system Al/WTi/CrSi/SiO2) [16]. The quantitative result is limited by the roughness of the sample (from preparation and ion induced), by interface artefacts and the general non-accuracy of the crater-profilometer measurement. Nevertheless, the differences of the sputter rates of the first two layers (Al and WTi) are clearly visible. The interfaces are characterized by peaks in the sputter rates (new implantation steady state). Whereas on the base of such results the computer simulation of depth profile measurement is possible, the aim of the computation of the concentration-depth-distribution from the measurements is still not reached.

5 Investigation of chemical states

Investigation of chemical states is the field of the electron spectroscopies (AES, XPS). The following example shows the application of principal components analysis to detect different peak shapes in depth profiles. The investigations were directed to surface modifications by ion implanta-

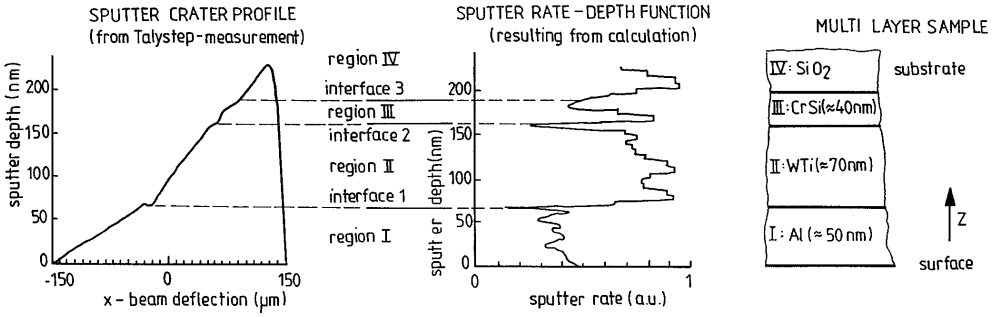

Fig. 6 Calculated sputter rate-depth function from a wedge crater experiment of an Al/WTi/CrSi/SiO_2 multilayer system (primary ions $^{16}O_2^+$, normal incidence, 18.5 keV)

tion of titanium implants for medical purposes [17]. We have investigated the depth distribution of phosphorus implanted in polished titanium at 20 keV with doses from $1 \cdot 10^{15}/cm^2$ to $3 \cdot 10^{17}/cm^2$ by AES and XPS [18].

Phosphorus was detected by AES for all doses. The depth profiles are given in Fig. 7. The native oxide layer on titanium is thinned with increasing ion dose. With doses $\geq 10^{17}/cm^2$ in the near-surface region, a P-rich phase is formed which contains ca. 20 % oxygen, and oxygen is enriched in the maximum implantation depth, probably due to O_2^+ implanted together with $^{31}P^+$. It was impossible to calibrate the depth scale by surface profilometry of sputter craters, because the sample roughness exceeds implantation and sputter depth. Calculations of the implantation parameters by means of the TRIM program yield a projected range for P in Ti of 25 nm and showed that under our conditions sputtering cannot be neglected. In the samples implanted with high doses, depth profiles of P($L_{2,3}$VV) peak displays change in shape and position (Fig. 8a). At low concentrations the detection of phosphorus is limited by noise. To analyze peak shapes, the P($L_{2,3}$VV) spectra recorded on all samples were evaluated by principal components analysis (PCA).

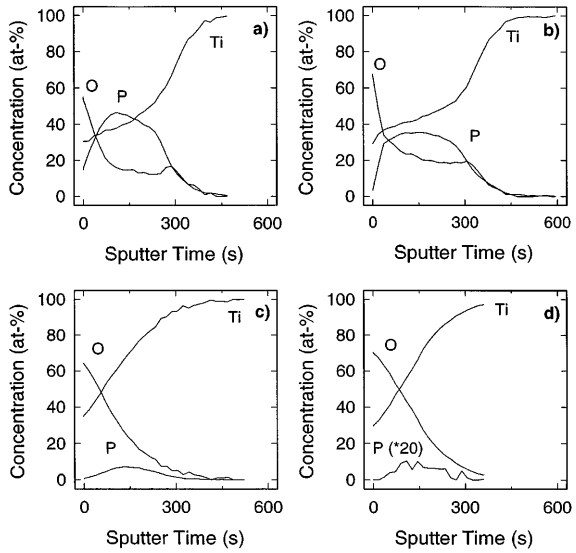

Fig. 7 AES depth profiles of titanium samples implanted with $^{31}P^+$ and sputtered by 4 keV argon ions. Ion dose: **a)** $3 \cdot 10^{17}/cm^2$; **b)** $1 \cdot 10^{17}/cm^2$; **c)** $1 \cdot 10^{16}/cm^2$; **d)** $1 \cdot 10^{15}/cm^2$

The principles of the method are summarized in [19]. Shortly, the data are assumed to be a linear combination of unknown basic spectra. They are determined by computing the eigenvalues of the data sets' covariance matrix. PCA assumes that large eigenvalues represent significant spectral information and small eigenvalues are connected with noise. Because the eigenvectors span an orthogonal space, their shape does not match the shape of the measured spectra (so-called abstract basic spectra). The linear combination of the basic spectra, however, restores the spectral shape. There is no exact criterion to distinguish between relevant spectral shapes and noise. The number of significant eigenvectors is determined using the magnitude or certain functions of the eigenvalues [19] and the precision of data reconstruction. Abstract basic spectra have to be transformed into spectroscopically relevant peak shapes by means of matrix rotation.

For our P($L_{2,3}$VV) data set we found three eigenvectors to be necessary (Fig. 8b) to keep the spectral information. The lines in Fig. 8a show how the reconstructed spectra fit the spectral shape. The separation of the spectral shape from noise by PCA is visible in the case of the smallest Auger peak. It should be noted here that this is an improvement in signal-to-noise ratio without a-priori information (models, peak shapes, standard spectra) or filter functions.

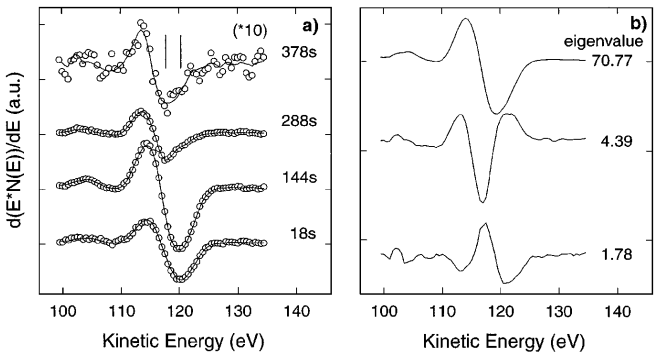

Fig. 8a, b Characteristic peak shapes of P($L_{2,3}$VV) Auger electron spectra. **a)** Spectra recorded on the sample implanted with $3 \cdot 10^{17}/cm^2$ P ions after the displayed sputter times (*circles*) and the result of data reconstruction using 3 eigenvectors (*lines*). The different peak positions at 117.5 and 119.5 eV are marked. **b)** Shape of the most prominent orthonormal eigenvectors. The numbers are the eigenvalues

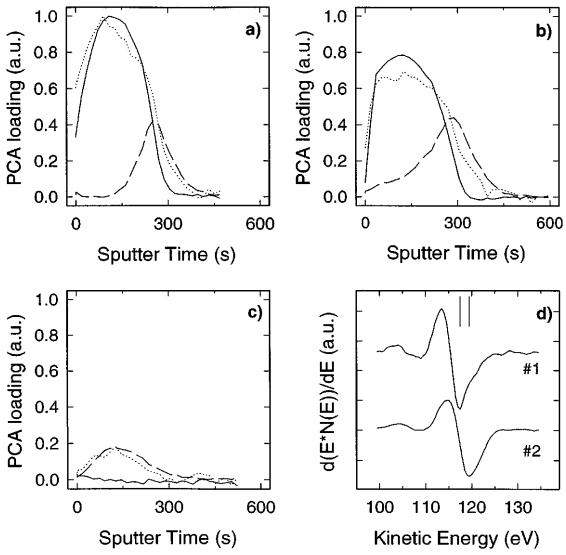

Fig. 9a–d Result of principal components analysis of the phosphorus Auger transitions. Depth profiles of the P(KLL) transition (*dotted*) and the two main components of the $P(L_{2,3}VV)$ transition attributed to interstitial P (*broken line*) and a TiP-like phase (*solid line*). Ion dose: **a)** $3 \cdot 10^{17}/cm^2$; **b)** $1 \cdot 10^{17}/cm^2$; **c)** $1 \cdot 10^{16}/cm^2$; **d)** Basic spectra of the $P(L_{2,3}VV)$ Auger transitions attributed to interstitial P (#1) and the TiP-like phase (#2). The different peak positions at 117.5 and 119.5 eV are marked

Rotation of the abstract basic spectra produced two P-rich spectra (Fig. 9d). For the weaker P(KLL) transition only one peak shape was found. The depth profiles of both $P(L_{2,3}VV)$ components together with P(KLL) are shown in Fig. 9a–c. The first component displays a distribution similar to an implantation profile. When the ion dose is increased from $1 \cdot 10^{16}/cm^2$ to $1 \cdot 10^{17}/cm^2$, the maximum is found after a longer sputter time. This is the depth where the sample is enriched in oxygen bound to titanium. The second component appears in the surface region for doses $\geq 10^{17}/cm^2$. When the ion dose is increased from $1 \cdot 10^{17}/cm^2$ to $3 \cdot 10^{17}/cm^2$, the amount of this phase increases, partially at the expense of the area under the first curve, whereas the maximum intensity of the first component remains constant. The single P(KLL) component behaves like the sum of both components. XPS depth profiles on the samples implanted with $1 \cdot 10^{16}/cm^2$ and $3 \cdot 10^{17}/cm^2$ ions showed differences in the P 2p photoelectron peak. It can be assumed that at higher concentrations Ti-P bonds are formed. Using small TiP single crystals as a standard, both AES and XPS showed that the surface layer is similar to TiP, but contained a certain amount of implanted oxygen. From the pure elements TiP is formed only at high temperature (about 900° C [20]). A certain amount of P, however, remains on interstitial sites in a depth similar to the ion range, i.e. in the region of maximum lattice distortion. For P implanted in Ti at high energy (130 keV, $5 \cdot 10^{16}/cm^2$), no significant shift of the P 2p peak compared to TiP is observed [20, 21]. For the titanium Auger and photoelectron peaks only small variations were found. Because changes of the spectral shape appear only in the $P(L_{2,3}VV)$ transition and not in the peaks involving only core levels (P(KLL) Auger and P 2p photoelectron), we conclude that this is caused by differences in the valence band structure of bound and interstitial phosphorus.

6 Cross-section analysis with the analytical TEM

A special technique for thin layer depth profiling is the analytical TEM, which allows section imaging and analysis by EDXS and by EELS after a complicated sample preparation [22]. As an example, Fig. 10a shows a Cr-Fe-multilayer system, where the imaging electrons sustained characteristic energy losses at the ionization edges of layer atoms [23]. The broad bands reflect the density of electrons with a characteristic energy loss of 574 eV (Cr L-

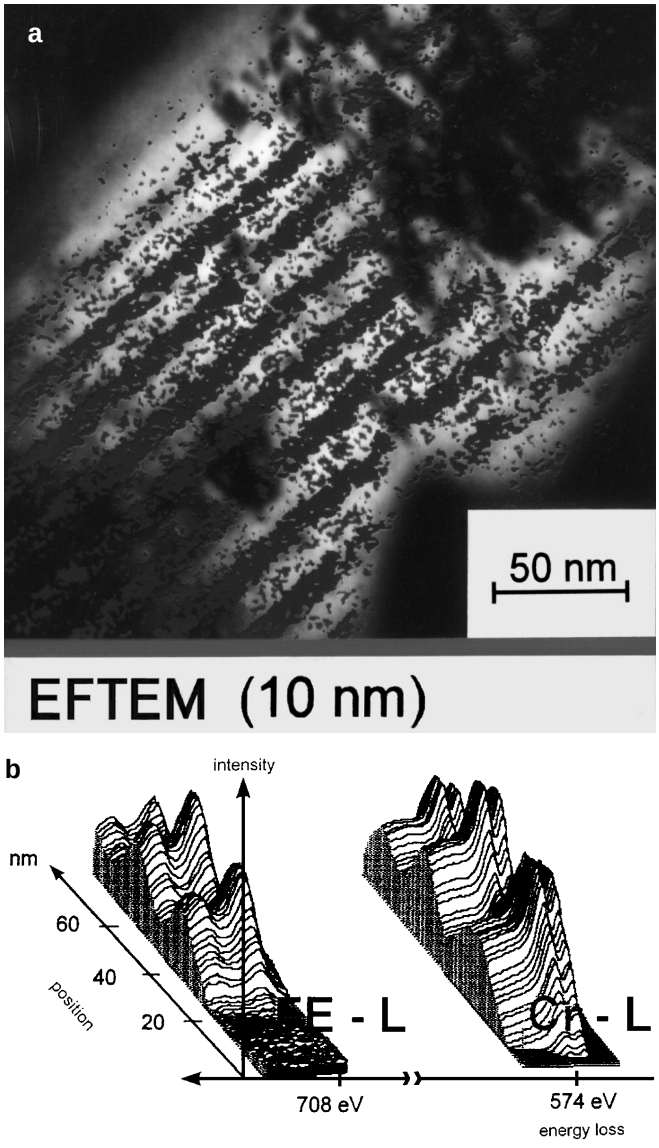

Fig. 10a, b Analytical electron microscopic investigation of a Cr-Fe multilayer system. **a)** Energy selected imaging of the Cr and Fe layers; **b)** Energy loss spectra by parallel EELS technique

edge); that means they depict Cr layers with 11 nm thickness. The smaller speckled bands are Fe layers with 8 nm thickness. The depth resolution of all other profiling methods is here immediately visible as lateral resolution. Further analysis of the depth profiles is possible by the simultaneous registration of energy loss spectra with parallel EELS technique (Fig. 10b). Besides the intensity peaks characterizing the L ionization edges of Fe and Cr, respectively, one can see a fine structure which provides knowledge on chemical bonding of the individual layer [24, 25]. This method passes through a rapid process of development, and in future it will contribute to interesting results in the field of quantitative depth profiling of thin layer systems.

References

1. Linsmeier Ch (1994) Vacuum 45:673
2. Boumans PWJM. (1972) Anal Chem 14:1219
3. Hofmann S (1990) Practical Surface Analysis 1:143
4. Behrisch R (1981) Sputtering by Particle Bombardment I. Springer, Berlin Heidelberg New York
5. Behrisch R (1983) Sputtering by Particle Bombardment II. Springer, Berlin Heidelberg New York
6. Behrisch R, Wittmaack K. (1991) Sputtering by Particle Bombardment III. Springer, Berlin Heidelberg New York
7. Hofmann S (1984) In: Oechsner H (ed) Thin film and depth profile analysis. Springer 37:141
8. Magee CW, Honig RE (1982) Surface and interface analysis 4:35
9. Bengtson A (1985) Spectrochim Acta B40:631
10. Präßler F, Hoffmann V, Schumann J, Wetzig K (1996) Fresenius J Anal Chem 355:840
11. Hoffmann V, Ehrlich G (1995) Spectrochim Acta B50:607
12. Wucher A, Oechsner H (1989) Fresenius Z Anal Chem 333:474
13. Voigtmann R, Moldenhauer W (1988) Surf Interface Anal 13: 167
14. Oswald S, Voigtmann R (1989) Proc 12th ICXOM, Cracow, 1:336
15. Oswald S, Hoffmann V, Ehrlich G. (1994) Spectrochim Acta 49B:1123
16. Oswald S (1991) Proc. 8th Int. Conf. SIMS VIII, Amsterdam, Abstract book, p 175
17. Ohtsuka Y (1993) Proc. 8th Int. Conf. Surface Modification of Metals by Ion Beam Dynamic Mixing, Kanazawa/Japan, p 72
18. Baunack S, Oswald S., Scharnweber D (in preparation)
19. Malinowski ER, Howery DG (1980) Factor Analysis in Chemistry. Wiley, New York Chichester Brisbane Tokyo
20. Myers CE, Franzen HF, Anderegg JW (1985) Inorg Chem 24:1822
21. Ferdjani S, David D, Beranger G, Farkas G, Hild S, Garcia EA (1991) J Alloys Compounds 177:265
22. Wetzig K, Bauer H-D (1996) Fresenius J Anal Chem 355:447
23. Mensch A (1995) Private communication
24. Robards AW (1993) Procedures in Electron Microscopy. Wiley, Chichester
25. Krivanek OL, Paterson JH (1990) Ultramicroscopy 32:313